# Kinetics of Low-Pressure, Low-Temperature Graphene Growth: Toward Single-Layer, Single-Crystalline Structure

**Hamid Mehdipour and Kostya (Ken) Ostrikov***

CSIRO Materials Science and Engineering, Plasma Nanoscience Centre Australia (PNCA), P.O. Box 218, Lindfield, New South Wales 2070, Australia, and Plasma Nanoscience @ Complex Systems, School of Physics, University of Sydney, New South Wales 2006, Australia

**ABSTRACT** Graphene grown on metal catalysts with low carbon solubility is a highly competitive alternative to exfoliated and other forms of graphene, yet a single-layer, single-crystal structure remains a challenge because of the large number of randomly oriented nuclei that form grain boundaries when stitched together. A kinetic model of graphene nucleation and growth is developed to elucidate the effective controls of the graphene island density and surface coverage from the onset of nucleation to the full monolayer formation in low-pressure, low-temperature CVD. The model unprecedentedly involves the complete cycle of the elementary gas-phase and surface processes and shows a precise quantitative agreement with the recent low-energy electron diffraction measurements and also explains numerous parameter trends from a host of experimental reports. These agreements are demonstrated for a broad pressure range as well as different combinations of precursor gases and supporting catalysts. The critical role of hydrogen in controlling the graphene nucleation and monolayer formation is revealed and quantified. The model is generic and can be extended to even broader ranges of catalysts and precursor gases/pressures to enable the as yet elusive effective control of the crystalline structure and number of layers of graphene using the minimum amounts of matter and energy.

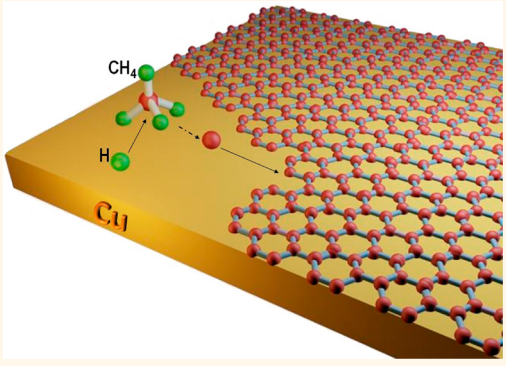


**KEYWORDS:** graphene · elementary surface processes · nucleation · graphene coverage

Owing to its exceptional mechanical, electronic, chemical, and optical properties, single-layer graphene is highly promising for high-frequency nanoelecronics,[1−3] biosensing,[4] flexible electronics,[5] and a plethora of other applications.[6,7] However, several requirements both in terms of the material quality and the fabrication technique need to be met to materialize these promises. Metal-catalyzed chemical vapor deposition (CVD) has recently been widely accepted as a viable approach toward graphene synthesis.[8−19] Indeed, it combines the advantages of high-quality, large-area graphene films with the possibility to produce them at relatively low temperatures directly in the specified device locations or transfer to other (*e.g.*, flexible) substrates depending on the envisaged applications.

Ultimately, the graphene film should have a single-layer, single-crystalline, and defect-free structure over the entire catalyst surface. However, this is extremely difficult to achieve, especially when using metal catalyst layers with low solubility of carbon.[20] In this case, graphene islands nucleate and grow by surface attachment of carbon atoms and form graphene grains. These grains have different orientations and form grain boundaries when stitched together.[21] Moreover, since carbon atoms are mostly produced by catalytic decomposition on the metal surface, it becomes increasingly difficult to complete the monolayer as the surface coverage increases. Hydrogen-assisted dissociation of hydrocarbon precursors has been shown to be very effective for ensuring a continued supply of carbon atoms under these and also many other carbon-starving

* Address correspondence to kostya.ostrikov@csiro.au.

Received for review September 8, 2012 and accepted October 19, 2012.

**Published online October 19, 2012**
**10.1021/nn3041446**

conditions. Moreover, the presence of certain amounts of hydrogen is needed to initiate and then complete the monolayer formation.[10] However, the exact mechanisms of the hydrogen-assisted graphene nucleation and growth on metal catalysts still remain unclear.[10]

This is why numerical modeling of graphene nucleation, grain formation, and catalyst surface coverage is indispensable. However, due to the overwhelming complexity and the very large number of elementary processes involved in the creation, redistribution, and incorporation of carbon atoms into graphene clusters and networks, it is very challenging and effortful to develop the models which include all of these processes on one hand and use real-world experimental parameters on the other. The existing approaches commonly either use numerical simulations which rely on own parameters and time scales or select a certain subset of (*e.g.*, gas-phase or surface) processes to model a specific growth stage (*e.g.*, nucleation or grain formation).[16,22−28]

A reliable test of the viability of such modeling approaches would be the degree of quantitative agreement with the available experimental results. However, the previous attempts to describe the process of graphene layer formation do not quantify the kinetics of the surface coverage and also show significant discrepancies with the experimental results, in particular, in the evolution of carbon density on the surface.[29] The most likely reason is in the intrinsic difficulty to select the set of the gas-phase and surface processes that are most important under the specific experimental conditions. For example, modeling of the very low-pressure growth of good-quality, yet multigrain, graphene did not include the crucial kinetic processes of carbon precursor delivery from the gas phase, carbon atom production, and redistribution between the islands as well as carbon evaporation from the surface. This is why only some selected experimental trends in the evolution of carbon concentration on the surface in limited process parameter ranges can presently be reproduced, while significant quantitative discrepancies between the experimental and the modeling results remain.[29] The major disaccord is in the recovery of the observed nonmonotonic dynamics in the carbon atom concentration during the graphene nucleation and growth and, moreover, the differences in these dynamics in different temperature and pressure ranges.

Therefore, such models cannot reliably describe the graphene nucleation and growth, especially under varied process conditions such as higher pressures and other hydrocarbon precursors. The existing models also fail to explain and quantify the role of hydrogen in the experimentally observed nonmonotonic dependence of graphene surface coverage on hydrogen content.

Here we present a kinetic model of graphene nucleation and growth which resolves the above issues and can be applicable for a broader range of catalyst materials and precursor gases. This model describes the graphene growth process in its entirety, from nucleation of small carbon clusters up to the full monolayer coverage. This model very successfully describes the very low-pressure graphene growth on Ir and Ru catalysts using ethylene ($C_2H_4$) precursor, under low temperatures. More importantly, the results show excellent quantitative agreement with the experimental results during (both for the carbon surface concentration and graphene surface coverage) the entire graphene formation process, which testifies the high degree of reliability of the model. Building upon this positive test, the model is extended to describe the similar process under the low-pressure, low-temperature conditions using Cu catalyst and $CH_4 + H_2$ precursor. In this case, the modeling results are also consistent with numerous experimental results and allow one to quantitatively explain the effects of hydrogen on the nucleation and growth of graphene grains. These results suggest that our model is generic and can be either directly applied or straightforwardly adjusted for a large number of hydrocarbon precursors, catalyst materials, and also broad pressure ranges. Moreover, the model makes it possible to optimize the experimental process parameters to achieve full surface coverage by the smallest possible number of large single 2D graphene crystals, thereby nearing the solution of the ultimate problem of the atom- and energy-efficient growth of single-layer, single-crystalline graphene.

## RESULTS AND DISCUSSION

**Gas−Surface Interactions in Metal-Catalyzed Graphene Growth.** We consider the metal catalyst-assisted growth of the monolayer graphene using very low- and low-pressure thermal CVD of $C_2H_4/H_2 + CH_4$ gas mixture on Ru/Ir and Cu catalyst layers.[10,30,31] Figure 1 shows a large variety of the elementary surface processes involved in metal-catalyzed growth of graphene, such as thermal/hydrogen-induced dissociation of hydrocarbon molecules (building unit (BU) production), formation of C clusters, surface diffusion, and ripening of graphene islands, *etc.* The surface C atom (BU) production and loss are the primary processes in graphene growth (especially at low pressures when the surface reactions are considered as the rate-limiting step in graphene growth)[12] and strongly depend on the process parameters as well as on the choice of the catalyst layer, either Ru (Ir)[30,32] or Cu.[10,33] Besides C atoms (monomers), *ab initio* studies showed that carbon dimers can also be considered as viable building units for the graphene nucleation and growth[34] because they are (like C monomer) also mobile species on the Cu surface and can form larger C clusters prior to the formation of graphene nuclei. The BUs (C monomers)

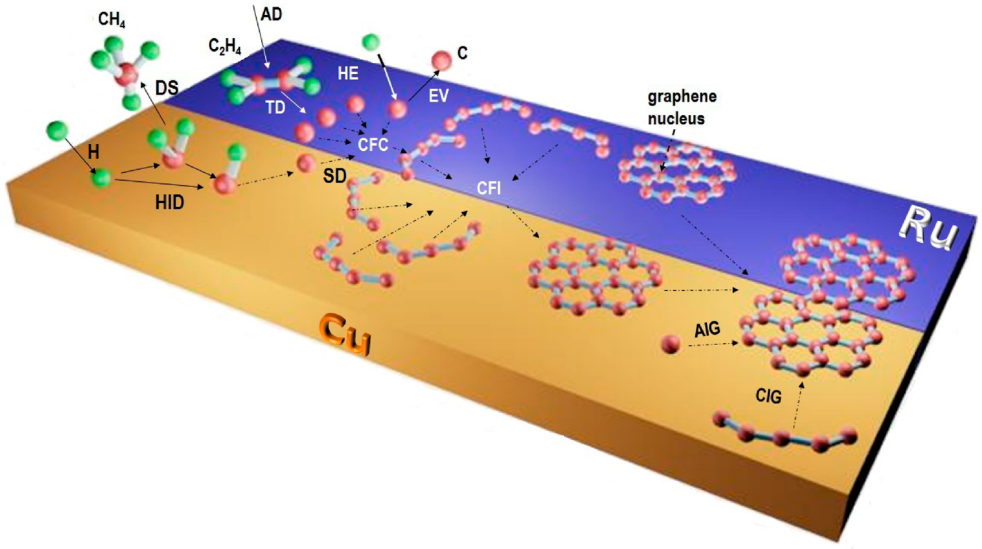


**Figure 1. Neutral gas−surface interactions as well as surface mechanisms involved in the nucleation and growth of monolayer graphene on Ru/Cu substrate in very low/low-pressure thermal CVD experiment in $C_2H_4/H_2 + CH_4$ gas mixtures. The most important surface processes involved in carbon atom production and graphene formation are thermal dissociation (TD), hydrogen-induced dehydrogenation (HID), adsorption of species (AD), desorption of species (DS), evaporation of carbon atoms (EV), surface diffusion of species (SD), C atom collisions and formation of 5-C atom cluster (CFC), cluster collisions and formation of graphene nuclei (CFI), stitching of graphene nuclei, and incorporation of carbon atom (AIG) and cluster (CIG) into the graphene structures.**

that remain on the surface diffuse and agglomerate to form (five C atoms) clusters,[30] which then diffuse and collide with each other, forming the initial graphene nuclei.[29,35] The five-C atom clusters are very important C species not only on Ru (Ir) surfaces but also on a Cu surface. Incorporation of these clusters to the zigzag edges (of the graphene nuclei) is a crucial step (providing stable binding sites for the following attachment of C monomers) in the growth of graphene islands in size.[16] However, the rates of monomer attachment to a graphene nucleus are expected to be higher than the rates of 5-atom cluster attachment. Otherwise, irregularly shaped graphene islands are expected, which contradicts the experimental observations[14,16] It is worth mentioning that the size of the initial graphene nuclei (5 × 6 C atoms) considered here, on both Ru (Ir) and Cu surfaces, is the closest nucleus size to the sizes of stable $C_{21}$ and $C_{24}$ nuclei (on metal catalyst layers, including Cu) predicted by *ab initio* calculations and also observed in experiments.[24]

After nucleation of the first graphene islands (with maximum density $n_l^{nuc}$), the islands start to diffuse and stitch to each other (Smoluchowski ripening),[35] thus forming larger graphene domains with a lower density. This process, which is strongly dependent on the temperature and the average distance between the islands ($n_l^{-1/2}$),[36] and incorporation of C precursors (C monomers and C clusters) into graphene network continue until the bare catalyst surface is fully covered by the graphene monolayer.

With increasing the catalyst temperature $T$, the thermal decomposition of hydrocarbon species (thus production of C) becomes more effective, which in turn leads to more BUs generated on the surface (hence nucleation takes place at a larger concentration; *i.e.*, $n_C^{nuc}$ increases). As a result, more (5-atom) clusters are formed (and then collide with each other), and more graphene nuclei nucleate on the metal surface (*i.e.*, $n_l^{nuc}$ increases with $T$) within much shorter times. However, further increasing in $T$ gives rise to more effective desorption/evaporation of precursor molecules/BUs, so nucleation time ($t_n$) increases, whereas $n_C^{nuc}$ decreases. Also, with increasing the hydrocarbon pressure $P_H$, one can expect the graphene nucleus density ($n_l^{nuc}$), graphene growth rate ($R_G$), and total graphene surface coverage ($\theta_G$) to increase, as well.

One should note that on some metal catalysts (*e.g.*, a Cu foil), several processes (*e.g.*, thermal decomposition or hydrogen/oxygen-assisted dehydrogenation) are responsible for the production of the BUs, and their relative importance depends on the temperature conditions[37] or the presence of other catalyst reactants (such as hydrogen and oxygen atoms).[37,38] On Cu metal substrates, direct thermal decomposition of hydrocarbon molecules (like $CH_4$ molecules on Cu surface) is energetically unfavorable,[27] or the rates of C generation (through the thermal decomposition) are very low.[37,38] This is why increasing the dose of exposure of the catalyst surface to hydrocarbon precursor is ineffective in promoting the graphene nucleation. Under these conditions, sufficiently high amounts of other catalytic agents, such as hydrogen atoms (supplied during the growth step or preadsorbed during annealing in hydrogen),[39,40] are required to

**TABLE 1. Elementary Surface Processes Included in the Model of Graphene Growth on Ru/Ir and Cu Substrates and Their Energy Activation Barriers (S and g Are Surface and Gas in the Reaction Notations Below)**

| surface processes | energy activation barriers |
|---|---|
| **adsorption** | |
| (1) $C_2H_{4(g)} \rightarrow C_2H_{4(S)}$ | (ZAE)[a] |
| (2) $CH_{4(g)} \rightarrow CH_{4(S)}$ | (ZAE) |
| (3) $H_{(g)} \rightarrow H_{(S)}$ | (ZAE) |
| **thermal dissociation** | |
| (4) $C_2H_{4(S)} \rightarrow 2C_{(S)} + 2H_{2(g)}$ | $E_{tdCH} = 1.87$ eV[9] |
| **desorption** | |
| (5) $C_2H_{4(S)} \rightarrow C_2H_{4(g)}$ | $E_{desCH} = 1.9$ eV[48] |
| (6) $CH_{4(S)} \rightarrow CH_{4(g)}$ | $E_{desCH} = 6.0$ eV[9] |
| (7) $H_{(S)} \rightarrow H_{(g)}$ | $E_{desH} = 1.9$ eV[49] |
| **hydrogen-induced reactions** | |
| (8) $C_2H_{4(S)}/CH_{4(S)} + H_{(g)} \rightarrow C_2H_{4(g)}/CH_{4(g)}$ | $E_{sdH} = 1.7$ eV[b] |
| (9) $C_{(S)} + H_{(g)} \rightarrow C_{(g)}$ | ~1.7 eV[b] |
| (10) $H_{(S)} + H_{(g)} \rightarrow H_{2(g)}$ | ~1.7 eV[b] |
| (11) $C_{(S)} + H_{(S)} \rightarrow CH_{(S)}$ | ~1.7 eV[b] |
| **C evaporation** | |
| (12) $C_{(S)} \rightarrow C_{(g)}$ | $E_{ev} = 3.25$ eV for Ru/Ir<br>=5.5 eV for Cu[9] |
| **dehydrogenation** | |
| (13) $CH_{4(S)} + H_{(S)} \rightarrow CH_{3(S)} + H_{2(g)}$ | $E_{sdH} = 1.7$ eV[b] |
| (14) $CH_{3(S)} + H_{(S)} \rightarrow CH_{2(S)} + H_{2(g)}$ | ~1.7 eV[b] |
| (15) $CH_{2(S)} + H_{(S)} \rightarrow CH_{(S)} + H_{2(g)}$ | ~1.7 eV[b] |
| (16) $CH_{(S)} + H_{(S)} \rightarrow C_{(S)} + H_{2(g)}$ | ~1.7 eV[b] |
| **surface diffusion of** | |
| carbon monomers | $E_{sdC} = 0.92$ eV for Ru/Ir[50]<br>= 0.1 eV for Cu[9] |
| 5-C atom clusters | $E_{sdCL} = 0.82$ eV[b] |
| graphene islands | $E_{sdIS} = 2.6$ eV[11] |
| **incorporation of** | |
| carbon monomers | $E_{incC} = 0.99$ eV for Ru/Ir[50]<br>= 0.85 eV for Cu[22] |
| carbon clusters | $E_{incCL} = 0.4$ for Ir/Ru[50]<br>= 0.8 eV for Cu[22] |

[a] Zero activation energy. [b] Optimized energy values.

produce enough BUs for the graphene nucleation through the reactions summarized in Table 1. However, further increasing the hydrogen content results in more effective etching of the precursor species and BUs from the surface (reactions 8 and 9 in Table 1). Consequently, the graphene growth rate decreases,[10,19] and the surface is then covered only partially or with a smaller number of graphene layers.[41] This effect becomes more pronounced at higher temperatures when the surface reaction between carbon and H atoms (reaction 11 in Table 1) becomes more effective. More details about the modeled mechanisms of graphene nucleation and growth and the assumptions made can be found in the Methods section and Supporting Information.

Our strategy in this work is based on taking into account the most important surface processes, thus

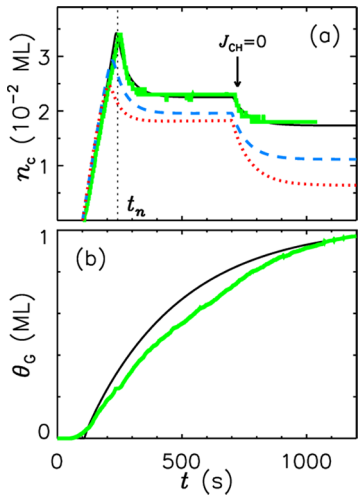


**Figure 2. Comparison of the experimental and numerical results on the nucleation and growth of a graphene monolayer on the Ru catalyst layer. The carbon atom concentration on the surface (a) and surface coverage (b) *versus* time from our modeling (black solid, dashed, and dotted curves) and LEEM measurements of Loginova *et al.*[31] (green, bold-solid curves). The solid, dashed, and dotted curves in (a) correspond to $T = 1020$, 900, and 800 K, respectively, while other input parameters are $P_{CH} = 3 \times 10^{-6}$ mTorr for (a) and $T = 1020$ K and $P_{CH} = 3 \times 10^{-5}$ mTorr for (b), which are exactly the same as the experimental values.[31]**

providing a comprehensive, yet simple, model to quantify the most important aspects of the graphene growth on a metal catalyst in CVD experiments. On one hand, this numerical modeling provides us with more insights into the base mechanisms of monolayer graphene formation during the entire growth process. On the other hand, our modeling results reproduce the main trends and are in good quantitative agreement with the numerous relevant experimental reports on CVD of graphene.[8−11,15,17−19,30−32,35,42−44] Importantly, these experiments have produced highly uniform, highly crystalline graphene films with the electrical characteristics comparable or even superior to mechanically exfoliated graphene films.[8,17,44]

**Numerical Results and Experimental Support.** Here we present the results of our numerical modeling of metal-catalyzed CVD graphene growth under (1) very low- and (2) low-pressure conditions. The relevant experimental observations that further validate our numerical model are discussed. Further details about the model and computation, such as assumptions, elementary surface processes, as well as more evidence about the suitability of our model to explain and quantify a variety of experimental results, can be found in the Methods section and Supporting Information.

**Very Low-Pressure Graphene Growth on Ru and Ir.** The results in Figure 2 pertain to all stages of the graphene synthesis, namely, the hydrocarbon gas exposure, graphene nucleation (Figure 2a), and the graphene growth and complete coverage of Ru catalyst surface by a monolayer graphene (Figure 2b). Figure 2a shows

the temporal evolution of the BU surface concentration during the precursor gas exposure as well as after the precursor gas supply is switched off ($J_{CH} = 0$). There is a very clear quantitative agreement between our numerical calculations and the experimental measurements by Loginova *et al.*[31] This agreement supports the choice of the appropriate set of basic equations and the elementary processes taken into account in our numerical model. A less detailed account of the BU production and losses during the graphene previously resulted in very significant discrepancies with the experimental measurements.[29] The very long nucleation time $t_n$ corresponds to the very long delays in the graphene nucleation at very low pressures ($3 \times 10^{-6}$ mTorr) observed experimentally. It is clearly seen that the nucleation time increases with substrate temperature $T$. However, $t_n$ decreases when $T$ is increased in the low-temperature range (see Figure S1 in the Supporting Information). This trend, which is rather unexpected, can be explained by noting that, with increasing $T$, thermal evaporation/desorption of BUs/hydrocarbon molecules becomes more effective. This in turn results in a decrease of BU surface density, which results in much longer time needed to nucleate graphene nuclei. However, increasing $T$ in the low-temperature range leads to more effective dissociation of precursor molecules (thus BU production rate increases). Consequently, the graphene nucleation starts much sooner (see Figure S1). Similar nonmonotonic numerical trends with increasing the catalyst temperature are observed (and compared with the data from LEEM measurements)[31] for C atom concentrations during the nucleation stage ($n_C^{nuc}$) and in equilibrium with the graphene domains ($n_C^{eq}$) (see Figure S2). The computed nonmonotonic trends perfectly reproduce the results from the LEEM measurements during graphene growth using ethylene precursor.[31] This is the first model which allows one to precisely quantify the nonmonotonic dynamics of carbon density on the Ru surface observed experimentally.

Figure 2b shows the numerically calculated time evolution of total graphene coverage $\theta_G(t)$, which has been superimposed with the experimental data from Figure 3 of Loginova *et al.*[31] corresponding to exposure of Ru substrate to ethylene precursor of a higher pressure (10 times larger than the pressure in panel (a)). Besides the clear recovery of the evolution trend of the measured surface coverage, the numerical data precisely overlap the experimental points at the beginning as well as when the graphene layer almost completely covers the surface. Only small quantitative discrepancies can be seen at intermediate growth stages, while the trend is still reproduced very well. These small discrepancies might have appeared because of the approximate incorporation barrier energies used in the calculations. It can be seen that, while the rate of the graphene coverage increase is high at the beginning, it then decreases as time elapses. This rate is nearly zero (see also Figure 3c) when the surface is almost completely covered by the graphene ($\theta_G \sim 1$). This is because, when the graphene islands grow in size and cover the metal surface, smaller bare metal areas are accessible for hydrocarbon molecules. Consequently, the adsorption (and then decomposition) of precursor molecules becomes less effective. Therefore, the BU production is weakened when the metal surface coverage by graphene increases. This leads to lower (or even zero) growth rates when the full coverage is reached. The computed coverage trend proves the primary role of thermal decomposition in the production of building material (required for continued graphene growth) and is also in good agreement with the experimentally measured decrease of the rates of the covered area change when the graphene covers more and more of the metal surface.[31]

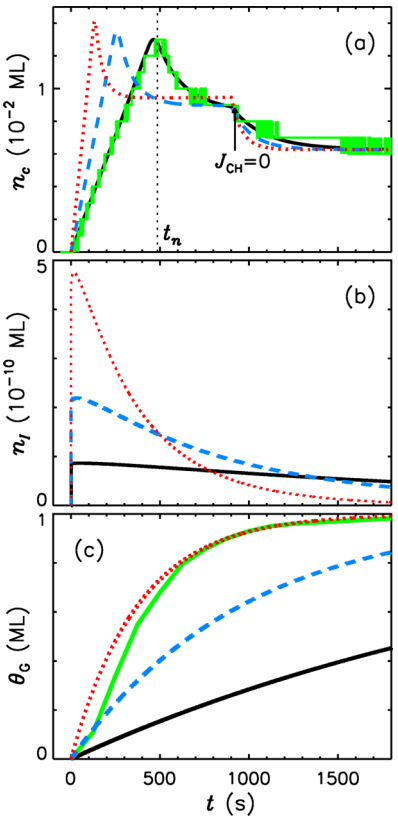


**Figure 3. Numerically quantified evolution of the graphene nucleation parameters and comparsion with the experimental results of graphene growth on the Ir catalyst layer. Carbon atom concentration (a), graphene island density (b), and graphene surface coverage (c) *versus* time from the solution of the complete set of rate equations (black solid, dashed, and dotted curves) and LEEM measurements (bold, green solid curves) of Loginova *et al.*[31] (in panel (a)) and Gastel *et al.*[32] (in panel (c)). The solid, dashed, and dotted curves in (a) correspond to $P_{CH} = 8 \times 10^{-7}$, $1.5 \times 10^{-6}$, and $3 \times 10^{-6}$ mTorr, respectively, while the same curves in panels (b) and (c) correspond to $P_{CH} = 10^{-5}$, $3 \times 10^{-5}$, and $7.5 \times 10^{-5}$ mTorr, respectively. Temperature is $T = 1100$ K in (a) and $T = 1210$ K in (b) and (c). Also, $t_n$ in (a) indicates the nucleation time which decreases as $P_{CH}$ is increased.**

The carbon monomer concentration on Ir is plotted in Figure 3a as a function of time and compared with the C concentration measured using LEEM technique under exactly the same temperature and pressure conditions ($T$ = 1100 K and $P_{CH} = 8 \times 10^{-7}$ mTorr). Again, it is clearly seen that not only the numerical solution reproduces all of the main features of the experimental data but also the numerical data completely overlap the experimental points. Figure 3a also highlights the strong dependence of the nucleation time $t_n$ on the hydrocarbon gas pressure ($P_{CH}$). The nucleation time decreases with increasing $P_{CH}$. This is because, with increasing the pressure, the flux of hydrocarbon molecules to the surface increases, thus more hydrocarbon molecules adsorb and undergo thermal decomposition on the surface. As a result, more BUs are produced, which in turn gives rise to faster saturation of the surface with carbon atoms. Consequently, cluster formation becomes more effective, thus the C cluster concentration increases, which in turn enables faster nucleation of graphene nuclei.

Changing the hydrocarbon pressure ($P_{CH}$) also affects both nucleation of graphene nuclei/islands and their subsequent growth in size. The effects of variation in $P_{CH}$ on graphene island density $n_I$ and graphene coverage $\theta_G$ are shown for three different hydrocarbon pressures ($P_{CH} = 10^{-5}$, $3 \times 10^{-5}$, and $7.5 \times 10^{-5}$ mTorr) in Figure 3b,c, respectively. These results suggest that Smoluchowski ripening accounts for the large drop in the island density at a higher $P_{CH}$ over the growth process duration (see Figure 3b). This can be explained by the very rapid increase of the nucleus density $n_I^{nuc}$ at the early stage of the graphene growth due to the increase of hydrocarbon pressure. Since the graphene nuclei are located closer to each other at high pressure, there would be a higher chance for the nuclei to easily diffuse and stitch to each other, thus producing larger islands with much lower surface density. The island density drop at high pressures is so large that the island density at high pressures is lower than at low pressures. This conclusion is exactly the same as the experimentally observed decrease of the graphene island density when the precursor gas dose is increased.[15]

The strong dependence of the graphene surface coverage on the precursor pressure is clearly seen in Figure 3c, where the numerical data are compared with the LEEM measurements during the CVD graphene growth experiment by Gastel *et al.*[32] under similar process conditions used in the modeling. The good quantitative agreement between the numerical and experimental results is achieved through a rigorous solution of a complete set of rate equations for the key species and several elementary surface processes. The increase of the total metal surface coverage (by graphene) with increasing $P_{CH}$ can be understood by noting that at higher pressures more hydrocarbon molecules are available on the surface. Hence, carbon

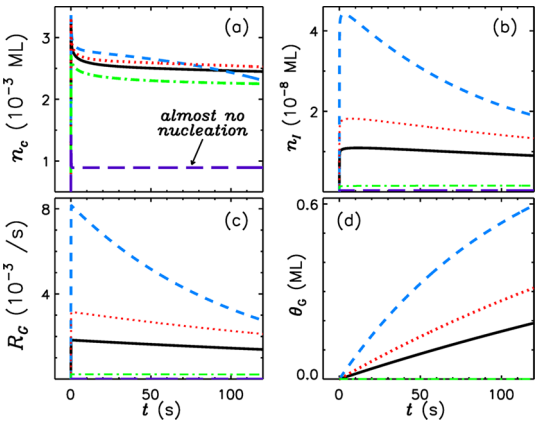


**Figure 4. Quantified important role of hydrogen gas in the nucleation and growth of a graphene layer in low-pressure CVD: carbon concentration (a), graphene island density (b), graphene growth rate (c), and graphene coverage (d) *versus* time at different hydrogen gas pressures with $T$ = 823 K and $P$ = 10 mTorr as default parameters. Long-dashed, dash-dotted, solid, dashed, and dotted curves correspond to $P_H$ = 0.05, 0.1, 0.2, 1.25, and 9.0 mTorr, respectively.**

monomer generation, and hence cluster formation, becomes more effective. As a result, more carbon monomers and clusters are available on the surface and can contribute to the graphene growth. The decrease of the graphene growth rate is more significant at higher hydrocarbon pressures, which further confirms the importance of metal-catalyzed thermal decomposition of precursor molecules on the bare area of the catalyst surface.

**Low-Pressure, Hydrogen-Induced Graphene Growth on Copper.** To illustrate the importance of hydrogen gas, we have modeled the effects of hydrogen atoms on the graphene nucleation and growth when copper (Cu) foil and methane ($CH_4$) are used as a metal catalyst and a precursor gas, respectively. As Figure 4a displays, it is intriguing to see that the carbon concentration does not reach the concentration threshold ($n_c^{nuc}$) required for the nucleation at very low hydrogen gas pressures, whereas it reaches this threshold value at higher $P_H$ even though $n_c^{nuc}$ also increases with increasing $P_H$. This is a numerical manifestation of the critical role of hydrogen atoms in BU production, thereby catalyzing graphene nucleation/growth. This effect reported experimentally by Vlassiouk *et al.*[10] remained unexplained theoretically until now. At higher hydrogen pressures, $n_c^{nuc}$ shows the opposite trend and decreases when the hydrogen pressure increases further. The absence of nucleation on a Cu surface exposed to $CH_4$ at very low hydrogen pressures can be understood by noting that thermal decomposition of $CH_4$ molecules is an endothermic process on the copper surface.[27] Thus, this process may act as a rate-limiting step and eventually hinder the graphene growth. This is why additional catalytic reactant, such as hydrogen, is needed to activate the dissociation of precursor molecules and thus provides a new channel for the effective production

of BUs required for the graphene nucleation (see Table 1).[45] After injecting the hydrogen gas into the chamber, the hydrogen molecules undergo thermal dissociation into hydrogen atoms. The generated hydrogen atoms adsorb on the surface and then diffuse and react with hydrocarbon species. These reactions lead to hydrogen-induced dissociation of hydrocarbon species to generate new species with fewer hydrogen atoms (see Table 1). This is why hydrogen gas pressure $P_H$ must reach a threshold value to effectively produce the required amount of BUs (*e.g.*, by catalytically active hydrogen adsorbates) and then start the graphene nucleation. However, it is known that not only hydrogen atoms from the gas phase can etch carbon atoms (and many other species such as CH, $CH_2$, $CH_3$, *etc.*), but also adsorbed hydrogen atoms can react with carbon monomers. These etching reactions lead to a severe depletion of BUs (required for nucleation/growth) at a very high $P_H$ and eventually suppression of the graphene nucleation. It must be mentioned that the hydrogen−BU reaction becomes more effective at higher temperatures when the surface diffusion of hydrogen atoms is enhanced and they can easily interact with the BUs.

This strong dependence of the Cu-catalyzed graphene nucleation on the hydrogen pressure is quantified in Figure 4a. It is clearly seen that graphene nucleation does not happen until the hydrogen pressure reaches a threshold pressure ($P_H^{th}$ = 0.1 mTorr). The C concentration initially increases with increasing $P_H$ and then drops with a further increase of the hydrogen pressure (see also Figure S3). The nonmonotonic behaviors of the growth rate and graphene nucleus density plotted in Figure 4b,c manifest the dual role of the hydrogen atoms in the graphene growth. The trends obtained numerically are in a reasonable agreement with the experiments that reported no graphene growth at very low hydrogen pressures and nonmonotonic change in the graphene growth with increasing the hydrogen content from low to very high pressures.[10] Chae *et al.* also reported no graphene growth at two extremes of hydrogen partial pressures (*i.e.*, no addition of hydrogen and very high dilution of hydrocarbon gas in $H_2$) in the gas mixture used in Ni-catalyzed growth of graphene.[41] The nonmonotonic change in the graphene island density with increasing $P_H$ as well as a smaller number of graphene nuclei at higher hydrogen pressures (see Figure 4b) also agrees very well with the experimental results.[10,11] The decrease of graphene growth rate with increasing $H_2$ concentration was also reported by Gao *et al.*,[19] which further validates our numerical results suggesting lower growth rates at very high $P_H$ (see Figure 4c). Therefore, hydrogen-assisted CVD is a viable approach to control the size and uniformity of graphene domains on the metal catalyst surface.[10]

Figure 4d shows the total surface coverage $\theta_G$ (by graphene) *versus* time at different hydrogen partial pressures. An increase of $\theta_G$ with increasing $P_H$ up to a certain threshold and the opposite trend at higher pressures indicate the importance of hydrogen pressure as a promising factor in controlling the graphene film thickness. By looking at Figure 4d, one can see that at a very high hydrogen pressure ($P_H$ = 9m Torr) the total graphene coverage ($\theta_G$) is smaller compared to $\theta_G$ at medium $P_H$ values. On one hand, this implies that the full surface coverage by graphene is unlikely to happen under high hydrogen pressures (see Figure S5), which is in very good agreement with experiments.[10] On the other hand, a high hydrogen pressure can be used to prevent the formation of the second or third graphene layers over the synthesis time expected for the formation of bi- or trilayer graphene under low-hydrogen pressure conditions. This possibility was demonstrated in the CVD of graphene, where the film thickness (number of layers) was reduced by increasing the hydrogen-to-hydrocarbon gas ratio.[41,46] It should be noted that our numerical model can predict the moment of completion of a single monolayer growth. This knowledge can be used to prevent the formation of bi- and trilayer graphene films, thereby producing a high-quality monolayer graphene.

The graphene grain (island) density and total surface coverage have also been calculated and then plotted for an intermediate value of hydrogen gas pressure and different hydrocarbon pressures and catalyst temperatures (see Figure 5a−d). The results obtained are compared with the observations of different experimental works on CVD-based growth of monolayer graphene. The increase of the graphene nucleus density $n_l^{max}$ at the nucleation stage with increasing hydrocarbon pressure ($P_{CH}$) and the temperature (from a low to an intermediate temperature) [panels (a) and (b)] can be

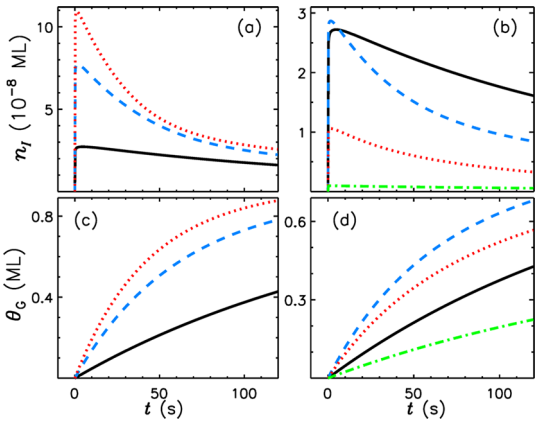


**Figure 5. Time evolution of the graphene island density (a,b) and the graphene surface coverage (c,d) under different pressures and temperatures. Solid, dashed, and dotted curves in (a) and (c) correspond to $P_{CH}$ = 1.0, 2.0, and 6.0 mTorr, respectively. Solid, dashed, dotted, and dash-dotted curves in (b) and (d) correspond to $T$ = 823, 873, 923, and 1023 K, respectively. Unless varied in any particular plot, the default set of parameters is $T$ = 823 K, $P$ = 10 mTorr, $P_H$ = 1.25 mTorr, and $P_{CH}$ = 1.0 mTorr.**

attributed to the generation of larger numbers of carbon atoms (and thus formation of more C clusters) at higher $P_{CH}$ and $T$. This change of the graphene nucleus density with hydrocarbon pressure is consistent with the reported decrease of nucleation sites at lower the precursor pressures.[9]

As times elapses, the as-formed graphene nuclei diffuse and collide, thus forming graphene islands. The graphene islands can in turn diffuse and stitch together, thereby producing larger islands with a lower density. The decrease in the island density is more pronounced at higher $P_{CH}$ and $T$ over the same time periods (see Figure 5a,b). These numerical results suggest that, similarly to the very low-pressure case, the Smoluchowski ripening process is enhanced with increasing the island (nuclei) density at the early growth stages due to large numbers of C clusters formed (due to larger amounts of carbon monomers generated on the surface) under high hydrocarbon pressure and high-temperature conditions. The nonmonotonic change in the island density obtained numerically is in good agreement with the observed increase and then decrease of the graphene island density during the CVD growth on copper.[11] Also, the calculated smaller number of nuclei at low $P_{CH}$ and $T$ is very consistent with the smaller numbers of graphene nuclei observable in SEM images of the films grown at lower temperatures and pressures.[17,35,43] The results of our calculations in Figure 5b also suggest that higher temperatures (below the intermediate value, *i.e.*, $T = 873$ K, considered here) lead to lower graphene island densities, which is precisely confirmed by the experimental observations of the lower island densities at higher catalyst temperatures.[9,11,17,18]

It was also reported that the graphene growth rate decreases nonlinearly with the increase of the surface coverage by graphene.[17] The surface coverage in turn increases with the precursor gas pressure and catalyst temperature.[9,17] To explain these observations, Figure 5c,d (Figure S4) displays the surface coverage *versus* time (the graphene growth rate *versus* surface coverage) at different hydrocarbon pressures and substrate temperatures, respectively. As Figure 5c shows, the full surface coverage by graphene is possible only at reasonably high hydrocarbon partial pressures ($P_{CH}$ = 6 mTorr),[17] whereas the Cu surface still remains partially covered at low $P_{CH}$. This can be explained by the fact that the graphene growth rate becomes higher with increasing $P_{CH}$ due to more effective production of carbon BUs. As a result, the BU incorporation into the graphene network is enhanced, and eventually, much more area on the bare metal surface is covered by the graphene. It is also possible that (if the temperature is high enough) graphene nucleation and growth can take place on top of a single-layer graphene domain/sheet during the same growth cycle. Thus, an increase of the graphene film thickness can also be expected at higher hydrocarbon precursor pressures. Moreover, our results also suggest that the number of layers (in graphene domains) can be tuned effectively by simply adjusting the hydrocarbon gas pressure. This possibility has been confirmed by several experiments suggesting that increasing the hydrocarbon pressure leads to graphene domains with two or three layers, which compromises the uniformity of the graphene film.[10,42]

The nonmonotonic change in the total graphene coverage with increasing catalyst temperature $T$ manifests the strong interplay between the hydrogen-induced dissociation (HID) of precursor molecules and hydrogen−BU recombination and desorption processes (see Figure 5d). In the low-temperature range ($T$ < 900 K), increasing $T$ leads to more effective BU production (through more effective HID) and an increase of the graphene surface coverage, in good agreement with many experimental results.[9,17] However, with further increasing the temperature (and thus increasing the BU surface concentration), more BU−hydrogen reactions (effective hydrogen etching) take place on the catalyst surface. Besides, evaporation of C atoms (from the catalyst surface) and desorption of hydrocarbon species (prior to dehydrogenation) become more effective at high temperatures, which in turn leads to less C atoms present on the surface. Therefore, due to a decrease of the BU surface concentration ($n_C$), the graphene growth rate also decreases, which results in a smaller total surface area covered by the monolayer graphene. The strong temperature dependence of the rates of hydrogen etching and evaporation of BUs has previously been confirmed experimentally.[10,47] Indeed, there is a minimum temperature for the etching of graphene domains as well as evaporation/desorption of C atom/precursor species to become effective.[10,47] The hydrogen etching at high temperatures is so strong that full coverage of the metal surface by graphene is not possible even for much longer processes (see Figure S5). Moreover, a similar trend in the graphene coverage change with increasing the temperature was observed when only hydrocarbon precursor was used.[47] This is also consistent with the frequent observations that the catalyst surface still remains only partially covered by graphene while the growth of graphene domains stops after a long time into the CVD process.[9,10]

**Toward Large-Area, Highly Uniform, Highly Crystalline Graphene Films.** The results of our numerical experiments agree with the results of numerous graphene growth experiments conducted at very low or low pressures. We emphasize that our numerical results obtained for typical conditions of low-temperature CVD of graphene offer a simple practical approach to effectively control the grain density and uniformity of the graphene sheets. Importantly, this can be achieved while keeping the energy and matter usage to the minimum, thus nearing the goal of the as yet elusive matter- and

energy-efficient CVD synthesis of large-area, highly crystalline, uniform graphene layers. This is particularly important because of several advantages of CVD compared to many other techniques, such as sublimation and mechanical cleavage. These advantages include notably lower temperatures, the possibility of catalytic healing of graphene network, as well as fairly easy transfer of the as-grown graphene to other (*e.g.*, flexible) substrates.

Further numerical computations at different combinations of CVD process parameters can help experimentalists to obtain the optimum process conditions for the CVD growth of graphene sheets with the degrees of uniformity and crystallinity required for the specific applications. For example, recent low-pressure, low-temperature CVD experiments led to the growth of large-area, highly crystalline graphene sheets with the electrical responses superior to exfoliated graphene.[44] This was achieved by a relatively slower low-pressure CVD which, as our numerical results suggested, leads to the smaller number of graphene seeds at the nucleation stage and the subsequently full coverage of the metal surface by graphene. This results in a smaller number of graphene grains with potentially different orientations and, consequently, better overall crystallinity of the final graphene sheet. A very similar result was reported by a two-step CVD experiment which involved a low-pressure stage followed by a high-pressure step. The first step was used to minimize the number of graphene seeds, while the high-pressure step has led to a rapid coverage of the catalyst surface by a graphene monolayer of a very small number of grains boundaries.[17] These experiments proved the nucleation of a smaller number of graphene grains at low hydrocarbon pressures, which was also observed in our numerical experiments.

Since very similar dependencies of the density of graphene nuclei on other process parameters (*e.g.*, temperature and hydrogen pressure) were obtained in our numerical modeling and numerous experiments by other authors, we believe that predictive numerical parameter optimization would be indispensable to synthesize graphene monolayers with fewer grain boundaries across the layer surface. Therefore, on one hand, this work provides experimentalists with specific protocols in real process parameter space to customize the thermal CVD conditions to produce (at remarkably lower temperatures) very uniform, highly crystalline graphene films suitable for the envisaged applications. On the other hand, a broad range of the surface processes taken into account in our model and very good quantitative agreement of our numerical results with the experimental findings of other authors lead to a better understanding of the underlying elementary mechanisms of both graphene nucleation and growth under different process conditions.

## CONCLUSION

Our numerical results therefore explain and quantify the common experimental observations of metal-catalyzed growth of graphene layers in very low and low-pressure CVD experiments, where highly crystalline, large-area graphene layers can be grown at low temperatures.[8]

One of the main outcomes of this work is the achieved very good quantitative agreement with the experimental results in reasonably broad parameter ranges. We have also intimately related the temperature and gas-phase conditions to the precursor gas and metal catalyst used to initiate the nucleation of graphene. Our results have also explained the dual role of hydrogen in Cu-catalyzed graphene growth. We have also presented the results of detailed investigations of the process, showing the possibility of effective control of graphene growth parameters, such as the surface coverage, number of single-crystalline grains, number of layers, *etc.* Our systematic numerical study of the recent experimental advances in low-temperature CVD growth of epitaxial graphene on metal substrates explains a host of relevant experimental observations. It can also be used to further improve the process predictability and optimize the synthesis conditions for the growth of graphene layers with specific grain sizes and uniformity, which is highly desired for a broad range of applications.

## METHODS

**Overview and Main Assumptions.** We consider the metal catalyst-assisted nucleation and growth of the graphene layer in $C_2H_4/H_2 + CH_4$ gas mixtures commonly used in thermal CVD of graphene on metal substrates.[8,9] The model used accounts for the most essential elementary processes on the metal surface, such as species creation/loss, surface diffusion of species, formations of clusters and large graphene islands, *etc.*, in very low and low-pressure CVD of graphene. Figure 1 shows the schematics of the key species deposition, carbon atom generation processes, as well as C cluster/nuclei formation and their surface diffusion to form nuclei/graphene islands on a metal (Ru/Ir or Cu) substrates heated externally to temperature $T$. The carbon diffusion into the metal substrates is assumed to be negligible in the temperature range considered here. The carbon atoms are created on the top surface of a metal catalyst layer *via* thermal/hydrogen-induced decomposition (dehydrogenation) and then diffuse and attach to each other, forming 5-C atom clusters. It is assumed that each six 5-C atom clusters diffuse and collide, forming an initial graphene nucleus[29] which then diffuses and stitches to other nuclei (Smoluchowski ripening), thus producing a large graphene island.[36] The Smoluchowski ripening is more effective at higher temperatures as well as when a larger number of nuclei emerge on the metal surface at the early stage of growth. The monomer and cluster attachments to the graphene islands continue until the metal surface is fully covered by graphene. Thus, both monomer and cluster attachments contribute to the graphene growth, and their importance varies depending on the metal catalyst used.

When copper is used as a substrate and methane as a precursor gas, increasing the temperature as well as hydrocarbon and hydrogen pressures leads to the production of more carbon atoms on the metal surface, which in turn leads to more effective formation of C clusters. Consequently, much more graphene nuclei are nucleated on the surface; as a result, the distance between graphene nuclei becomes smaller. Consequently, diffusion and coalescence of graphene nuclei/islands becomes more effective, so larger islands with a lower density are formed and then grow rapidly in size by attachment of C monomers and C clusters. This in turn leads to faster coverage of the metal surface by the monolayer graphene. In this case, the probability of the nucleation and growth of the second layer also increases.

The set of graphene growth equations includes

$$\frac{dn_C}{dt} = J_C^+ - J_C^- \quad (1)$$

for the surface concentration of carbon atoms $n_C$ and

$$\frac{d\theta_G}{dt} = (m \times p) n_C^m \nu \quad \exp(-E_{sdCL}/kT) + n_{CL} n_{IS} \nu \quad \exp(-(E_{sdCL} + E_{incCL})/kT) + n_C n_{IS} \nu \quad \exp(-(E_{sdC} + E_{incC})/kT) \quad (2)$$

for the graphene surface coverage $\theta_G$, as well as appropriate equations for the key hydrogen and hydrocarbon species, C clusters, and graphene islands (see Supporting Information).

In eq 1, the first term, $J_C^+$, describes the production of the carbon atoms on the metal surface due to thermal decomposition of ethylene (on Ru/Ir catalyst) and methane (on Cu catalyst) molecules, hydrogen-induced dehydrogenation of CH radicals (on Cu substrate), as well as thermal dissociation of C clusters and graphene nuclei. The second term in eq 1, $J_C^-$, accounts for carbon atom loss due to evaporation, hydrogen-induced etching, C cluster formation, and C atom incorporation into the graphene grain structure. In eq 2, the first term describes the nucleation of the first graphene nuclei (due to surface diffusion of clusters (with energy barrier $E_{sdCL}$) and their agglomeration), while the second and third terms account for carbon monomer and cluster (diffusion and then) attachment to the graphene islands (with energy barriers, $E_{incC}$ and $E_{incCL}$, respectively. Here, $\theta_G$ is the graphene coverage, $m = 5/p = 6$ are the numbers of carbon atoms/clusters in a cluster/nucleus, $n_{CL}$ is the surface density of clusters, $n_{IS}$ is the surface density of graphene nuclei (islands), and $E_{sdC}$ is the energy barrier for C atom diffusion on the metal surface.

The hydrogen and hydrocarbon fluxes onto the bare metal surface are proportional to graphene-free surface area (*i.e.*, $1 - \theta_G$), so the species deposition onto the metal surface becomes less effective and eventually impossible as $\theta_G$ increases and approaches unity. As a result, the thermal processes of carbon atom creation become less effective with increasing the graphene surface area,[31] hence, fewer carbon atoms are produced, and thus the graphene growth slows down and eventually stops.

We emphasize that the model of graphene nucleation and island formation based on the predominant contributions of C monomers and 5-atom clusters presented in previous studies[29] (and in this work) has led to very good agreements between the numerical results and the experimental measurements of graphene growth on Ru/Ir and Cu catalysts.[30,31] However, incorporation of $m = 2, 3, 4$, *etc.* clusters is expected to make the model of graphene growth more generic and may help further improving the quantitative agreement with the available experimental results, especially for the Cu catalyst case.

*Conflict of Interest:* The authors declare no competing financial interest.

*Acknowledgment.* The authors would like to thank E. (Loginova) Starodub for providing the experimental data for the direct quantitative comparison with our numerical modeling results. This work was partially supported by the Australian Research Council and CSIRO's OCE Science Leadership Program. H.M. acknowledges support by the University of Sydney International Scholarship and CSIRO OCE top-up scholarship.

*Supporting Information Available:* The complete set of model equations and comprehensive descriptions and discussions of the processes taken into account, additional numerical results on the dependence of the graphene growth parameters on the process parameters, and their relevance to experimental measurements. This material is available free of charge *via* the Internet at http://pubs.acs.org.

## REFERENCES AND NOTES

1. Lin, Y.-M.; Dimitrakopoulos, C.; Jenkins, K. A.; Farmer, D. B.; Chiu, H.-Y.; Grill, A.; Avouris, P. 100-GHz Transistors from Wafer-Scale Epitaxial Graphene. *Science* **2010**, *327*, 662.
2. Wu, Y.; Lin, Y.-M.; Bol, A. A.; Jenkins, K. A.; Xia, F.; Farmer, D. B.; Zhu, Y.; Avouris, P. High-Frequency, Scaled Graphene Transistors on Diamond-like Carbon. *Nature* **2011**, *472*, 74–78.
3. Mueller, T.; Xia, F.; Avouris, P. Graphene Photodetectors for High-Speed Optical Communications. *Nat. Photonics* **2010**, *4*, 297–301.
4. Dan, Y.; Lu, Y.; Kybert, N. J.; Luo, Z.; Johnson, A. T. C. Intrinsic Response of Graphene Vapor Sensors. *Nano Lett.* **2009**, *9*, 1472–1475.
5. Bae, S.; Kim, H.; Lee, Y.; Xu, X.; Park, J.-S.; Zheng, Y.; Balakrishnan, J.; Lei, T.; Kim, H. R.; Song, Y.; *et al.* Roll-to-roll Production of 30-in. Graphene Films for Transparent Electrodes. *Nat. Nanotechnol.* **2010**, *5*, 574–578.
6. Novoselov, K. S.; Geim, A. K.; Morozov, S. V.; Jiang, D.; Zhang, Y.; Dubonos, S. V.; Grigorieva, I. V.; Firsov, A. A. Electric Field Effect in Atomically Thin Carbon Films. *Science* **2004**, *306*, 666–669.
7. Berger, C.; Song, Z.; Li, X.; Wu, X.; Brown, N.; Naud, C.; Mayou, D.; Li, T.; Hass, J.; Marchenkov, A. N.; *et al.* Electronic Confinement and Coherence in Patterned Epitaxial Graphene. *Science* **2006**, *312*, 1191–1196.
8. Li, X.; Cai, W.; An, J.; Kim, S.; Nah, J.; Yang, D.; Piner, R.; Velamakanni, A.; Jung, I.; Tutuc, E.; *et al.* Large-Area Synthesis of High-Quality and Uniform Graphene Films on Copper Foils. *Science* **2009**, *324*, 1312–1314.
9. Kim, H.; Mattevi, C.; Calvo, M. R.; Oberg, J. C.; Artiglia, L.; Agnoli, S.; Hirjibehedin, C. F.; Chhowalla, M.; Saiz, E. Activation Energy Paths for Graphene Nucleation and Growth on Cu. *ACS Nano* **2012**, *6*, 3614–3623.
10. Vlassiouk, I.; Regmi, M.; Fulvio, P.; Dai, S.; Datskos, P.; Eres, G.; Smirnov, S. Role of Hydrogen in Chemical Vapor Deposition Growth of Large Single-Crystal Graphene. *ACS Nano* **2011**, *5*, 6069–6076.
11. Hwang, C.; Yoo, K.; Kim, S. J.; Seo, E. K.; Yu, H.; Bir, L. P. Initial Stage of Graphene Growth on a Cu Substrate. *J. Phys. Chem. C* **2011**, *115*, 22369–22374.
12. Bhaviripudi, S.; Jia, X.; Dresselhaus, M. S.; Kong, J. Role of Kinetic Factors in Chemical Vapor Deposition Synthesis of Uniform Large Area Graphene Using Copper Catalyst. *Nano Lett.* **2010**, *10*, 4128–4133.
13. Zhang, B.; Lee, W. H.; Piner, R.; Kholmanov, I.; Wu, Y.; Li, H.; Ji, H.; Ruoff, R. S. Low-Temperature Chemical Vapor Deposition Growth of Graphene from Toluene on Electropolished Copper Foils. *ACS Nano* **2012**, *6*, 2471–2476.
14. Yu, Q.; Jauregui, L. A.; Wu, W.; Colby, R.; Tian, J.; Su, Z.; Cao, H.; Liu, Z.; Pandey, D.; Wei, D.; *et al.* Control and Characterization of Individual Grains and Grain Boundaries in Graphene Grown by Chemical Vapour Deposition. *Nat. Mater.* **2011**, *10*, 443–449.
15. Coraux, J.; N'Diaye, A. T.; Engler, M.; Busse, C.; Wall, D.; Buckanie, N.; Heringdorf, F.-J. M.; van Gastel, R.; Poelsema, B.; Michely, T. Growth of Graphene on Ir(111). *New J. Phys.* **2009**, *11*, 023006.
16. Luo, Z.; Kim, S.; Kawamoto, N.; Rappe, A. M.; Johnson, A. T. C. Growth Mechanism of Hexagonal-Shape Graphene Flakes with Zigzag Edges. *ACS Nano* **2011**, *5*, 9154–9160.
17. Li, X.; Magnuson, C. W.; Venugopal, A.; An, J.; Suk, J. W.; Han, B.; Borysiak, M.; Cai, W.; Velamakanni, A.; Zhu, Y.; *et al.* Graphene Films with Large Domain Size by a Two-Step Chemical Vapor Deposition Process. *Nano Lett.* **2010**, *10*, 4328–4334.

18. Wu, B.; Geng, D.; Guo, Y.; Huang, L.; Xue, Y.; Zheng, J.; Chen, J.; Yu, G.; Liu, Y.; Jiang, L.; *et al.* Equiangular Hexagon-Shape-Controlled Synthesis of Graphene on Copper Surface. *Adv. Mater.* **2011**, *23*, 3522–3525.
19. Gao, L.; Ren, W.; Zhao, J.; Ma, L.-P.; Chen, Z.; Cheng, H.-M. Efficient Growth of High-Quality Graphene Films on Cu Foils by Ambient Pressure Chemical Vapor Deposition. *Appl. Phys. Lett.* **2010**, *97*, 183109.
20. Gao, L.; Guest, J. R.; Guisinger, N. P. Epitaxial Graphene on Cu(111). *Nano Lett.* **2010**, *10*, 3512–3516.
21. Wei, Y.; Wu, J.; Yin, H.; Shi, X.; Yang, R.; Dresselhaus, M. The Nature of Strength Enhancement and Weakening by Pentagon−Heptagon Defects in Graphene. *Nat. Mater.* **2012**, *11*, 759–763.
22. Shu, H.; Chen, X.; Tao, X.; Ding, F. Edge Structural Stability and Kinetics of Graphene Chemical Vapor Deposition Growth. *ACS Nano* **2012**, *6*, 3243–3250.
23. Gao, J.; Yip, J.; Zhao, J.; Yakobson, B. I.; Ding, F. Graphene Nucleation on Transition Metal Surface: Structure Transformation and Role of the Metal Step Edge. *J. Am. Chem. Soc.* **2011**, *133*, 5009–5015.
24. Yuan, Q.; Gao, J.; Shu, H.; Zhao, J.; Chen, X.; Ding, F. Magic Carbon Clusters in the Chemical Vapor Deposition Growth of Graphene. *J. Am. Chem. Soc.* **2012**, *134*, 2970–2975.
25. Gao, J.; Yuan, Q.; Hu, H.; Zhao, J.; Ding, F. Formation of Carbon Clusters in the Initial Stage of Chemical Vapor Deposition Graphene Growth on Ni(111) Surface. *J. Phys. Chem. C* **2011**, *115*, 17695–17703.
26. Saadi, S.; Pedersen, F, A.; Helveg, S.; Sehested, J.; Hinnemann, B.; Appel, C. C.; Nørskov, J. K. On the Role of Metal Step-Edges in Graphene Growth. *J. Phys. Chem. C* **2010**, *114*, 11221–11227.
27. Zhang, W.; Wu, P.; Li, Z.; Yang, J. First-Principles Thermodynamics of Graphene Growth on Cu Surfaces. *J. Phys. Chem. C* **2011**, *115*, 17782–17787.
28. Neyts, E. C.; Shibuta, Y.; van Duin, A. C. T.; Bogaerts, A. Catalyzed Growth of Carbon Nanotube with Definable Chirality by Hybrid Molecular Dynamics-Force Biased Monte Carlo Simulations. *ACS Nano* **2010**, *4*, 6665–6672.
29. Zangwill, A.; Vvedensky, D. D. Novel Growth Mechanism of Epitaxial Graphene on Metals. *Nano Lett.* **2011**, *11*, 2092–2095.
30. Loginova, E.; Bartelt, N. C.; Feibelman, P. J.; McCarty, K. F. Evidence for Graphene Growth by C Cluster Attachment. *New J. Phys.* **2008**, *10*, 093026.
31. Loginova, E.; Bartelt, N. C.; Feibelman, P. J.; McCarty, K. F. Factors Influencing Graphene Growth on Metal Surfaces. *New J. Phys.* **2009**, *11*, 063046.
32. van Gastel, R.; N'Diaye, A. T.; Wall, D.; Coraux, J.; Busse, C.; Buckanie, N. M.; Meyer zu Heringdorf, F.-J.; Horn von Hoegen, M.; Michely, T.; Poelsema, B. Selecting a Single Orientation for Millimeter Sized Graphene Sheets. *Appl. Phys. Lett.* **2009**, *95*, 121901.
33. Rasool, H. I.; Song, B.; Mecklenburg, M.; Regan, B. C.; Wang, K. L.; Weiller, B. H.; Gimzewski, J. K. Atomic-Scale Characterization of Graphene Grown on Copper (100) Single Crystals. *J. Am. Chem. Soc.* **2011**, *133*, 12536–12543.
34. Riikonen, S.; Krasheninnikov, A. V.; Halonen, L.; Nieminen, R. M. The Role of Stable and Mobile Carbon Adspecies in Copper-Promoted Graphene Growth. *J. Phys. Chem. C* **2012**, *116*, 5802–5809.
35. Wang, B.; Ma, X.; Caffio, M.; Schaub, R.; Li, W.-X. Size-Selective Carbon Nanoclusters as Precursors to the Growth of Epitaxial Graphene. *Nano Lett.* **2011**, *11*, 424–430.
36. Stoldt, C. R.; Jenks, C. J.; Thiel, P. A.; Cadilhe, A. M.; Evans, J. W. Smoluchowski Ripening of Ag Islands on Ag(100). *J. Chem. Phys.* **1999**, *111*, 5157–5166.
37. Alstrup, I.; Chorkendorff, I.; Ullmann, S. The Interaction of $CH_4$ at high Temperatures with Clean and Oxygen Precovered Cu(100). *Surf. Sci.* **1992**, *264*, 95–102.
38. La Cava, A. I.; Bernardo, C. A.; Trimm, D. L. Studies of Deactivation of Metals by Carbon Deposition. *Carbon* **1982**, *20*, 219–223.
39. Tao, L.; Lee, J.; Chou, H.; Holt, M.; Ruoff, R. S.; Akinwande, D. Synthesis of High Quality Monolayer Graphene at Reduced Temperature on Hydrogen-Enriched Evaporated Copper (111) Films. *ACS Nano* **2012**, *6*, 2319–2325.
40. Lee, S.; Lee, K.; Zhong, Z. Wafer Scale Homogeneous Bilayer Graphene Films by Chemical Vapor Deposition. *Nano Lett.* **2010**, *10*, 4702–4707.
41. Chae, S. J.; Gunes, F.; Kim, K. K.; Kim, E. S.; Han, G. H.; Kim, S. M.; Shin, H.-J.; Yoon, S.-M.; Choi, J.-Y.; Park, M. H.; *et al.* Synthesis of Large-Area Graphene Layers on Poly-Nickel Substrate by Chemical Vapor Deposition: Wrinkle Formation. *Adv. Mater.* **2009**, *21*, 2328–2333.
42. Wu, W.; Yu, Q.; Peng, P.; Liu, Z.; Bao, J.; Pei, S.-S. Control of Thickness Uniformity and Grain Size in Graphene Films for Transparent Conductive Electrodes. *Nanotechnology* **2012**, *23*, 035603.
43. Liu, W.; Li, H.; Xu, C.; Khatami, Y.; Banerjee, K. Synthesis of High-Quality Monolayer and Bilayer Graphene on Copper Using Chemical Vapor Deposition. *Carbon* **2011**, *49*, 4122–4130.
44. Petrone, N.; Dean, C. R.; Meric, I.; van der Zande, A. M.; Huang, P. Y.; Wang, L.; Muller, D.; Shepard, K. L.; Hone, J. Chemical Vapor Deposition-Derived Graphene with Electrical Performance of Exfoliated Graphene. *Nano Lett.* **2012**, *12*, 2751–2756.
45. Lysaght, A. C.; Chiu, W. K. S. Modeling of the Carbon Nanotube Chemical Vapor Deposition Process Using Methane and Acetylene Precursor Gases. *Nanotechnology* **2008**, *19*, 165607.
46. Kim, Y.; Song, W.; Lee, S. Y.; Jeon, C.; Jung, W.; Kim, M.; Park, C.-Y. Low-Temperature Synthesis of Graphene on Nickel Foil by Microwave Plasma Chemical Vapor Deposition. *Appl. Phys. Lett.* **2011**, *98*, 263106.
47. Olle, M.; Ceballos, G.; Serrate, D.; Gambardella, P. Yield and Shape Selection of Graphene Nanoislands Grown on Ni(111). *Nano Lett.* **2012**, *12*, 4431–4436.
48. Hayashi, K.; Sato, S.; Ikeda, M.; Kaneta, C.; Yokoyama, N. Selective Graphene Formation on Copper Twin Crystals. *J. Am. Chem. Soc.* **2012**, *134*, 12492–12498.
49. Denysenko, I.; Ostrikov, K.; Cvelbar, U.; Mozetic, M.; Azarenkov, N. A. Carbon Nanofiber Growth in Plasma-Enhanced Chemical Vapor Deposition. *J. Appl. Phys.* **2008**, *104*, 073301.
50. Wu, P.; Jiang, H.; Zhang, W.; Li, Z.; Hou, Z.; Yang, J. Lattice Mismatch Induced Nonlinear Growth of Graphene. *J. Am. Chem. Soc.* **2012**, *134*, 6045–6051.